RAPID COMMUNICATION

Vapor cell geometry effect on Rydberg atom-based microwave electric field measurement*

Linjie Zhang(张临杰)[1,2,†], Jiasheng Liu(刘家晟)[1,2], Yue Jia(贾玥)[1,2], Hao Zhang(张好)[1,2], Zhenfei Song(宋振飞)[3], and Suotang Jia(贾锁堂)[1,2]

[1] *Institute of Laser Spectroscopy, State Key Laboratory of Quantum Optics and Quantum Optics Devices, Shanxi University, Taiyuan* 030006, *China*
[2] *Collaborative Innovation Center of Extreme Optics, Shanxi University, Taiyuan* 030006, *China*
[3] *National Institute of Metrology, Beijing* 100029, *China*

(Received 17 November 2017; revised manuscript received 1 January 2018; published online 13 February 2018)

The geometry effect of a vapor cell on the metrology of a microwave electric field is investigated. Based on the splitting of the electromagnetically induced transparency spectra of cesium Rydberg atoms in a vapor cell, high-resolution spatial distribution of the microwave electric field strength is achieved for both a cubic cell and a cylinder cell. The spatial distribution of the microwave field strength in two dimensions is measured with sub-wavelength resolution. The experimental results show that the shape of a vapor cell has a significant influence on the abnormal spatial distribution because of the Fabry–Pérot effect inside a vapor cell. A theoretical simulation is obtained for different vapor cell wall thicknesses and shows that a restricted wall thickness results in a measurement fluctuation smaller than 3% at the center of the vapor cell.

Keywords: Rydberg atom, microwave electric field strength, electromagnetically induced transparency (EIT), Aulter–Towns splitting

PACS: 32.80.Ee, 42.50.Gy, 84.40.–x **DOI:** 10.1088/1674-1056/27/3/033201

1. Introduction

The measurement of magnetic and electric fields using atoms and molecules has significant advantages of being linked to precision measurements of fundamental constants and atomic or molecular properties.[1–6] Precision measurement of microwave electric field (E-field) strength is important for wireless communications, remote sensing and antenna calibration.[6,7] The sensitivity of microwave E-field strength using classical dipole antennas is limited to 1 mV·cm^{-1}·Hz$^{-1/2}$ with an accuracy of 5%–20% and the traditional method cannot provide a traceable precise measurement of weak microwave E-fields. Rydberg atoms have been considered as a competitive option because the large-transition dipole moment between the energetically adjacent Rydberg states can be coupled by a microwave E-field. Many studies on microwave E-field measurement using the electromagnetically induced transparency (EIT) spectroscopy of Rydberg atoms have been performed.[5–13] Novel measurement methods have demonstrated high sensitivity,[5,8,9] the high resolution of E-field spatial distributions,[10–13] and the vector measurement of the RF E-field.[14] A new sensitivity of 5 μV·cm^{-1}·Hz$^{-1/2}$ was achieved using a homodyne detection technique.[8] The atomic vapor cell as a microwave E-field sensor plays a determining role for precise measurements. Compared to the conventional metal antenna, the dielectric atomic vapor cell introduces a weaker disturbance. The effect of the size of a cubic vapor cell was investigated in Ref. [15] and it was found that a cell size far smaller than the wavelength of microwave E-field (λ_{MW}) eliminated the Fabry–Pérot (FP) effect of the vapor cell and improved the measurement accuracy. In this study, the geometry effect of different vapor cell shapes on the measurement of microwave E-fields was investigated through the high resolution spatial distribution measurement of the microwave E-field inside vapor cells. A two-dimensional distribution of microwave E-fields was present. The experimental results showed that the FP effect inside a cylinder-shaped vapor cell was not greater than that of a cubic-shaped vapor cell when the size of vapor cells was greater than $\lambda_{\mathrm{MW}}/10$. The simulation of the E-field distribution in vapor cells with different wall thicknesses indicates that a thinner cell wall performs well for precise metrology.

2. Experimental approach

Figure 1(a) shows the atomic energy level scheme of our experiments. The cascade four-level system included a ground state $6S_{1/2}$, $F = 4(|1\rangle)$, an intermediate state $6P_{3/2}$, $F' = 5(|2\rangle)$, and Rydberg states $47D_{5/2}(|3\rangle)$ and $48P_{3/2}(|4\rangle)$. The transition frequency between the two Rydberg states was 6.946 GHz. A sketch of the experimental setup is shown in

*Project supported by the National Key Research and Development Program of China (Grant Nos. 2017YFA03044200 and 2016YFF0200104), the National Natural Science Foundation of China (Grant Nos. 91536110, 61505099, and 61378013), and the Fund for Shanxi "331 Project" Key Subjects Construction, China.

†Corresponding author. E-mail: zlj@sxu.edu.cn

Fig. 1(b). The probe light provided by an extended cavity diode laser (DL100, TOPTICA) with a wavelength of 852 nm was locked to a high-finesse glass ultra-stable cavity using the PDH technique. The estimated linewidth of the probe light was smaller than 30 kHz according to the cavity locking error signal of the reflective spectrum and the probe light frequency was tuned to the resonance transition of $6S_{1/2}, F = 4 \rightarrow 6P_{3/2}, F' = 5$ with an acoustic-optic modulator. The coupling light resonant with a transition of $6P_{3/2}, F' = 5 \rightarrow 47D_{5/2}$ was provided by a double-frequency laser system (TA-SHG pro, TOPTICA). The probe (coupling)-beam waist was 90 μm (100 μm) and power of 5.5 μW (25 mW). The probe laser was divided into two parallel beams and crossed the vapor cell to a differential photoelectric detector. One of the probe beams and the coupling beam with the same linear polarization were counter-propagated and coincided with each other inside the vapor cell. The atomic density was about 3.6×10^{10} cm^{-3} in the room-temperature vapor cell. The power of both lasers was stabilized using a feedback loop to acousto-optic modulators. The microwave E-field was produced with a signal generator (N5183B, Agilent) and fed to an atomic vapor cell with a standard-gain horn antenna (LB-180400-KF, A-INFO). The horn antenna was placed at a distance to the vapor cell to satisfy the far-field condition. The 6.946 GHz frequency microwave E-field coupled two nearby Rydberg state transitions of $47D_{5/2} \leftrightarrow 48P_{3/2}$. The transmission of the probe laser was detected by a fast differential photodetector and recorded using an oscilloscope when the frequency of the coupling laser was scanned. To avoid reflections of the microwave E-field from the experimental apparatus, microwave absorbers were placed around the vapor cell.

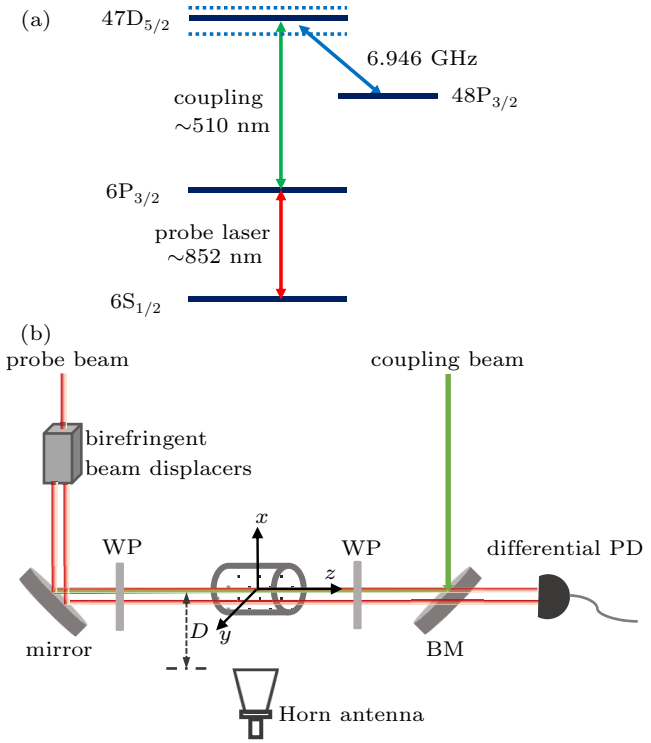

Fig. 1. (color online) Energy level scheme of Rydberg EIT with microwave E-field, (b) schematic of experimental setup. (WP:$\lambda/2$ wave plate, DM: dichroic mirrors). The specified coordinate system is shown in this figure. The propagation direction of microwave E-field is defined as the x-axis.

3. Results and discussion

The transmission signal and effect of the microwave E-field are shown in Fig. 2(a). The black solid line is a typical three-level EIT signature. The red dashed line shows the Aulter–Towns (AT) splitting signal effect on the microwave E-field. The microwave E-field strength E_{MW} is proportional to the Rabi frequency Ω_{MW} between $47D_{5/2}$ and $48P_{3/2}$ of the RF E-field and the frequency separation Δf_{P} of the splitting peaks and is calculated as

$$|E_{\mathrm{MW}}| = \frac{\hbar}{\wp_{\mathrm{MW}}}\Omega_{\mathrm{MW}} = 2\pi\frac{\hbar}{\wp_{\mathrm{MW}}}\Delta f_{\mathrm{p}}, \tag{1}$$

where $\wp_{\mathrm{MW}}$ is the transition dipole moment of $47D_{5/2} \leftrightarrow 48P_{3/2}$ and $\hbar$ is Planck's constant.[12] The AT splitting separations Δf_{P} were measured to represent the microwave E-field strength at the laser beam position. Here we used two typical atomic vapor cells with a saturated vapor pressure of ^{133}Cs one with a $30 \times 30 \times 30$ mm^3 cubic cell with 0.5 mm wall thickness and the other a cylinder cell 40 mm in length and 20 mm in diameter with 1.5-mm wall thickness.

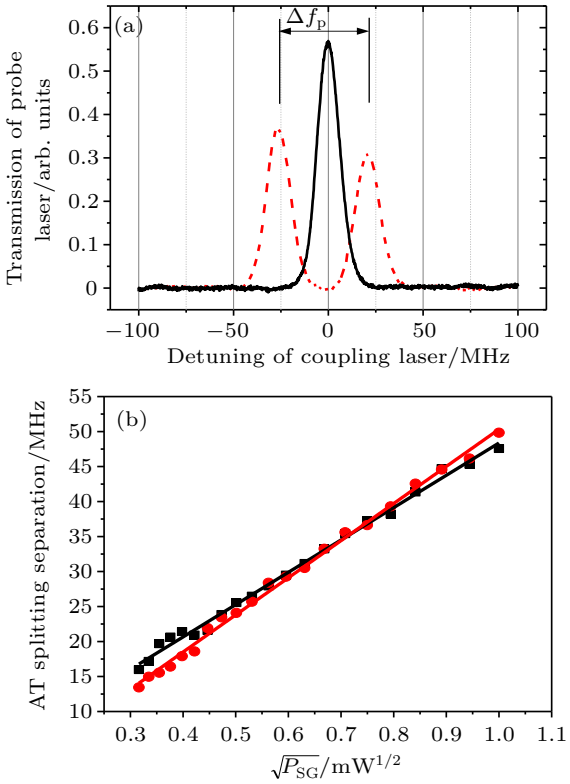

Fig. 2. (color online) (a) Transmission signal of probe laser (black solid line: without microwave E-field, red dashed line: with microwave E-field, Δf_{P} is the AT splitting separation), (b) dependence of AT-splitting separation on the square of power of microwave signal generator in two different vapor cells (black square: cubic cell, red circle: cylinder cell, solid lines: linear fitting results).

When the probe light and coupling light crossed the center of the square surface of the cubic cell and the axis of the cylinder cell, the dependence of $\Delta f_{\rm P}$ on the square of the power of the signal generator in different vapor cells was obtained as shown in Fig. 2(b). The solid lines in Fig. 2(b) are the linear fitting results. Taking into account the gain of the horn antenna and the insert loss of the cable, the microwave E-field strength was proportional to the square of the power of the signal generator. Figure 2(b) shows the linear relationship between the AT splitting separations and the microwave E-field strength. There was a slight difference in the measurement results in the center of the cubic- and cylindrical-shaped cells as shown in Fig. 2(b).

To clarify the effect of the geometry of a vapor cell, the microwave E-field distribution in two dimensions, parallel (x-axis) and perpendicular (y-axis) to the E-field propagation, was measured. The vapor cells were mounted on a three-dimensional translation stage with a 10-mm travel range. The position of the vapor cells to the laser beams was scannable with a precision of 0.01 mm. The spatial distribution of the microwave E-field strength was achieved by varying the position of the laser beam. The distribution of the microwave E-field strength for different x and y values is presented in Fig. 3. In Figs. 3(a) and 3(b), the E-field strength on the x-axis for $y = 3$, 0, and -3 mm are shown for the cylinder cell and cubic cell. The distribution of the E-field strength on the x-axis had similar features for small variations of y values. The monotone decay of the E-field strength in the cylinder cell was different than that of the cubic cell. The red solid lines in Figs. 3(a) and 3(b) are the simulation results for $y = 0$. Figures 3(c) and 3(d) show the E-field strength distribution on the y-axis for $x = -3$, 0, 3 mm that describe the wavefront plane of the microwave E-field. In the cylindrical cell, the E-field distribution in the wavefront plane fluctuated. The average E-field strength on the wavefront became smaller as the distance to the horn antenna increased. The strength distribution in the wavefront of the microwave E-field inside the cubic cell was very diverse. Taking into account the size of the vapor cell,[15] the ratio of the cell size to the microwave E-field wavelength was 0.69 for the cubic cell and 0.46 for the cylindrical cell. The symmetrical geometry of the cubic cell easily induced an FP effect in the x- and y-axis direction simultaneously.

The absorption of the vapor cell with a wall thickness d is described as[15]

$$\beta = 1 - \exp\left[-\frac{2\pi}{\lambda_{\rm MW}}\left(\frac{\delta d}{2}\right)\right], \tag{2}$$

which determines the absorption of the vapor cell to an E-field with a fixed wavelength. Here $\tan(\delta) = 0.005$ for the Pyrex

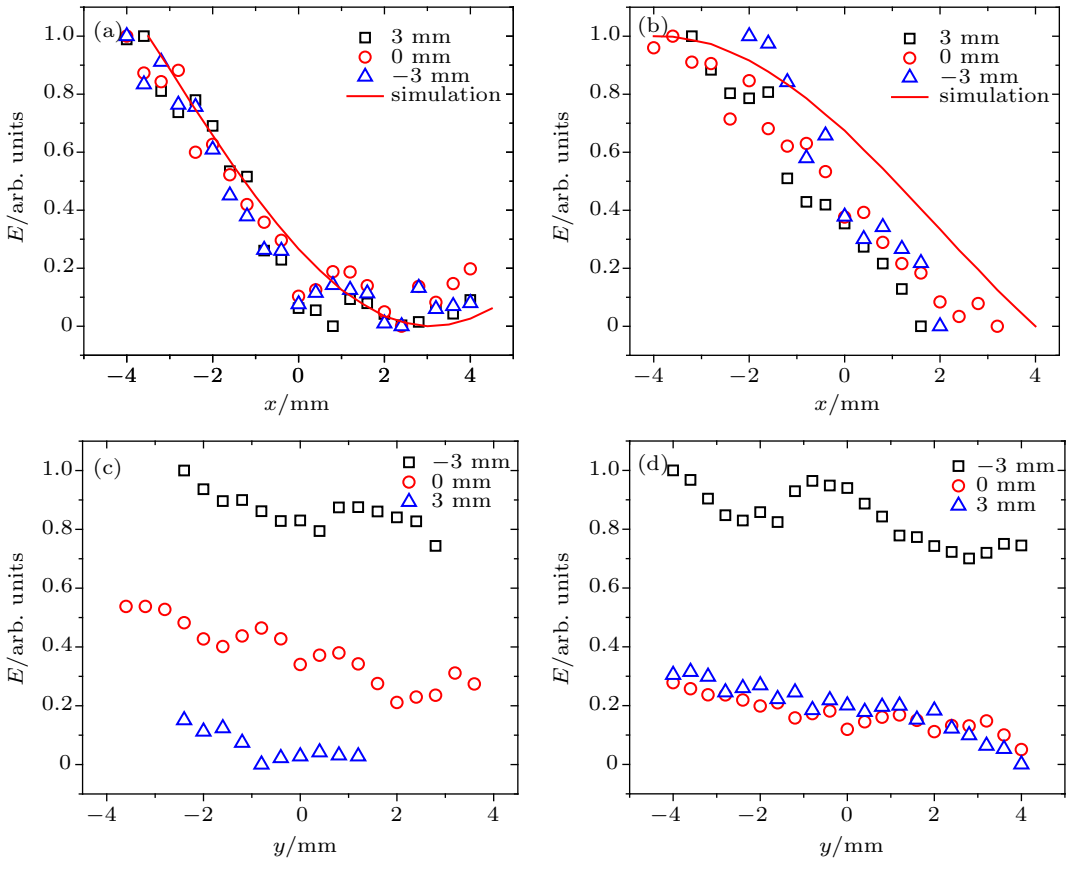

Fig. 3. (color online) Distribution of microwave E-field strength for (a) $y = 3$, 0, -3 mm at the x axis in the cylinder cell; (b) $y = 3$, 0, -3 mm at the x axis in the cubic cell; (c) $x = 3$, 0, -3 mm at the y axis in the cylinder cell; (d) $x = 3$, 0, -3 mm at the y axis in the cubic cell. The red solid lines are the theoretical simulation taking account of the thickness of vapor cell.

material.[16] For a 6.946-GHz microwave E-field, the absorption ratio of a 0.5-, 1-, and 1.5-mm vapor cell Pyrex wall is 0.018%, 0.036% and 0.055%, respectively. We used finite element analysis software to simulate the E-field strength distribution on the x-axis inside the vapor cells with wall thicknesses of 0.5, 1 and 1.5 mm as shown in Fig. 4. The green-star line in Fig. 4 is the E-field distribution without the vapor cell in accordance with the far-field feature of the microwave field $E_{\mathrm{MW}} \propto 1/R$ (R is the distance between the laser beam and the horn antenna). As shown a thinner wall has a weaker effect on the E-field strength at the center of the two vapor cells ($x = 0$). The cubic cell caused a smaller disturbance of the E-field distribution than the cylindrical cell at the x-axis. The vapor cell disturbance of the microwave E-field can be attributed to the reflection of the cell wall and the FP effect inside the cell. The thicker wall of the vapor cell resulted in a greater reflection of the E-field.

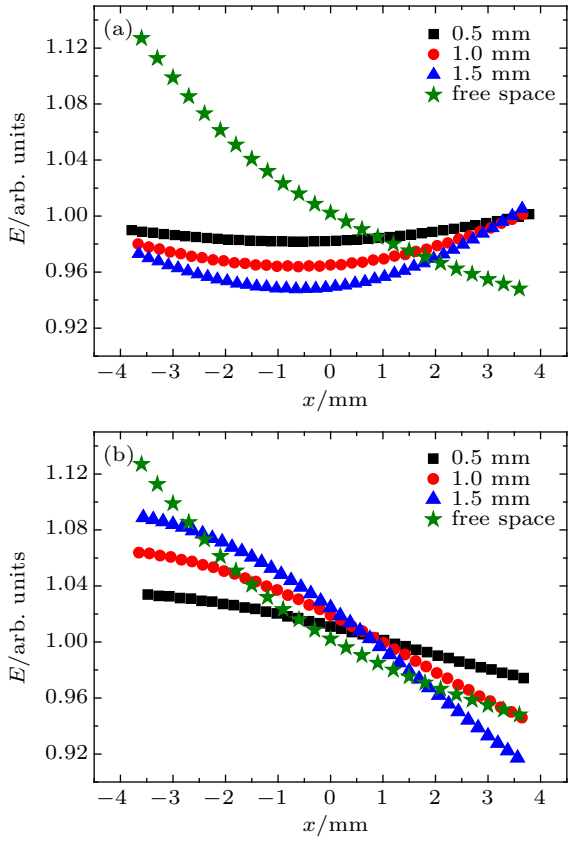

Fig. 4. (color online) Distribution of microwave E-field strength on x-axis for different wall thicknesses of (a) cylindrical cell and (b) cubic cell.

4. Conclusion

In this study, we investigated the geometry effect of a vapor cell on the metrology of a microwave E-field by splitting the EIT spectra of Rydberg atoms in a room-temperature cesium vapor cell. Two-dimensional high-resolution spatial distribution of the microwave E-field strength was achieved inside a cubic cell and a cylindrical cell. The spatial distribution on both the propagation direction and the wavefront of the microwave E-field was measured in different vapor cells. The experimental results show that vapor cell shape significantly influences the inhomogeneous spatial distribution because of the FP effect inside the vapor cell. Furthermore, the effect of vapor cell wall thickness on the precise measurement of microwave E-fields was considered. The theoretical simulation shows that a restricted wall thickness results in a measurement error smaller than 3% at the center of a vapor cell.

Acknowledgment

The authors acknowledge the fruitful discussion with Dr. Liyun Yan and Dr. Yuchi Zhang.

References

[1] Koschorreck M, Napolitano M, Dubost B and Mitchell M W 2010 *Phys. Rev. Lett.* **104** 093602
[2] Hanneke D, Fogwell S and Gabrielse G 2008 *Phys. Rev. Lett.* **100** 120801
[3] Savukov I M, Seltzer S J, Romalis M V and Sauer K L 2005 *Phys. Rev. Lett.* **95** 063004
[4] Horsley A and Treutlein P 2016 *Appl. Phys. Lett.* **108** 211102
[5] Sedlacek J, Schwettmann A, Kubler H, Low R, Pfau T and Shaffer J P 2012 *Nat. Phys.* **8** 819
[6] Kanda M 1994 *IEEE Transactions on Electromagnetic Compatibility* **36** 261
[7] Song Z, Feng Z, Liu X, Li D, Zhang H, Liu J and Zhang L 2017 *IEEE Antennas and Wireless Propagation Letters* **16** 1589
[8] Kumar S, Fan H, Kubler H, Sheng J and Shaffer J P 2017 *Sci. Rep.* **7** 42981
[9] Kumar S, Fan H, Kübler H, Jahangiri A J and Shaffer J P 2017 *Opt. Express* **25** 8625
[10] Fan H, Kumar S, Daschner R, Kubler H and Shaffer J P 2014 *Opt. Lett* **39** 3030
[11] Holloway C L, Gordon J A, Schwarzkopf A, Anderson D A, Miller S A, Thaicharoen N and Raithel G 2014 *Appl. Phys. Lett.* **104** 244102
[12] Zhou J, Zhang W Q, Hao Y M, Jin T, Jiang X H, Zhang H and Zhang L J 2016 *Journal of Quantum Optics* **22** 311 (in Chinese)
[13] Liu J S, Zhang H, Song Z F, Zhang L J and Jia S T 2016 *IEEE MTT-S International Conference Bei jing*, China, July 27–29, 2016
[14] Sedlacek J A, Schwettmann A, Kübler H and Shaffer J P 2014 *Phys. Rev. Lett.* **111** 063001
[15] Fan H Q, Kumar S, Sheng J T and Shaffer J P 2015 *Phys. Rev. Appl.* **4** 044015
[16] Westphal W B 1977 *Laboratory for Insulation Research, Massachusetts Institute of Technology Technical Report* No. AFML-TR-74-250